ACS APPLIED MATERIALS & INTERFACES

Research Article

Cite This: ACS Appl. Mater. Interfaces 2019, 11, 9530−9538

www.acsami.org

Biosensing with Insect Odorant Receptor Nanodiscs and Carbon Nanotube Field-Effect Transistors

Thanihaichelvan Murugathas,[†,‡,§] Han Yue Zheng,[†,‡] Damon Colbert,[∥] Andrew V. Kralicek,[∥] Colm Carraher,[*,∥] and Natalie O. V. Plank[*,†,‡]

[†]School of Chemical and Physical Sciences, Victoria University of Wellington, Wellington 6021, New Zealand

[‡]The MacDiarmid Institute for Advanced Materials and Nanotechnology, Wellington 6021, New Zealand

[§]Department of Physics, University of Jaffna, Jaffna 40000, Sri Lanka

[∥]The New Zealand Institute for Plant & Food Research Ltd., Auckland 1142, New Zealand

Supporting Information

ABSTRACT: Insect odorant receptors have been reconstituted into lipid nanodiscs and tethered to carbon nanotube field-effect transistors to function as a biosensor. Here, four different insect odorant receptors (ORs) from *Drosophila melanogaster* (DmelOR10a, DmelOR22a, DmelOR35a, and DmelOR71a) were expressed in Sf9 cells, purified, and reconstituted into lipid nanodiscs. We have demonstrated that each of these ORs produce a selective and highly sensitive electrical response to their respective positive ligands, methyl salicylate, methyl hexanoate, *trans*-2-hexen-1-al, and 4-ethylguaiacol, with limits of detection in the low femtomolar range. No detection was observed for each OR against control ligands, and empty nanodiscs showed no specific sensor signal for any of the odorant molecules. Our results are the first evidence that insect ORs can be integrated into lipid nanodiscs and used as primary sensing elements for bioelectronic nose technologies.

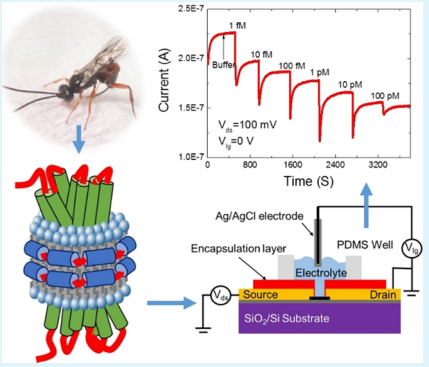

KEYWORDS: *Odorant receptors, Drosophila melanogaster, CNT network FET, Olfactory sensor, Electronic nose*

INTRODUCTION

Fast, selective, and on-site detection of odorant molecules at low concentrations is a critical challenge for health and safety, environmental monitoring, and food and water quality management.[1−5] Highly sensitive animal noses are widely used for detection of odorant molecules, with both insects and mammals involved in drug detection, biosecurity, search and rescue, and medical diagnostics.[6,7] However, there are drawbacks to using living animals for real-time detection, such as the cost and time associated with training and handling, interpretation of the response, and environmental and behavioral variation.[7] Recent research has demonstrated the potential for biosensors to mimic animal noses by coupling their odorant receptors (ORs) with a secondary signal transducer to form a biosensor.[2,8−10] Carbon nanotube field-effect transistors (CNT-FETs) are widely utilized as the signal transducer in biosensors because of their numerous advantages, such as low power consumption, smaller size, built-in signal amplification, and direct electrical readouts.[11−13]

Recently, mammalian ORs in combination with FET transducers have successfully detected odorant molecules at femtomolar concentrations.[1,14−20] However, although mammalian OR sensors have many excellent properties, there are some drawbacks. Mammalian ORs are G protein-coupled receptors (GPCRs), which require downstream signaling mechanisms in vivo to activate ion channels that then depolarize the neuron.[21] Inclusion of these downstream elements into a biosensor will be challenging, and without them, the sensor could have limited effectiveness. Also, mimicking a complete odorant sensing system requires the participation of all receptors present in the biological olfactory system. Theoretically, an array of sensors with multiple receptors is required to detect odorant molecules precisely. The large number of receptor proteins (∼400 in adult humans and ∼1700 in canines) in the mammalian odorant sensing system is another bottleneck in the design and implementation of a complete sensor array.[22,23]

Insect ORs, on the other hand, are members of a novel family of seven-transmembrane proteins that uniquely function as ligand-gated cation channels[24,25] and are a complex of an ion channel-forming subunit, odorant receptor co-receptor (Orco), and an odorant-binding receptor subunit, OR.[26,27] The OR subunit binds an odorant molecule in vivo, which then causes the Orco ion channel to open and results in an influx of ions. Although the signal transduction mechanism of the olfactory system in insects has not been fully identified, the role of ORs in converting the chemical signals from the odorant molecules into electrical signals during neurosignal transduction has been

Received: November 5, 2018
Accepted: February 11, 2019
Published: February 11, 2019

DOI: 10.1021/acsami.8b19433
ACS Appl. Mater. Interfaces 2019, 11, 9530−9538

confirmed.[25,27] Fruit flies have excellent sensitivity to odorant molecules, utilizing a family of approximately 60 ORs.[28−30] Many of these odorant receptors have been functionally characterized.[31−33] An adult fruit fly's olfactory system contains 45 functional ORs, and its larval olfactory system contains 21 functional ORs.[33,34] This means that an array of sensors with 45 different OR protein-functionalized channels would be sufficient to mimic the complete odorant sensory system of an adult fruit fly.

The basic principle behind CNT-FET olfactory sensors involves immobilizing the receptors on the sidewalls of CNTs to transduce the odorant-induced electrical changes. However, immobilizing membrane-bound proteins onto CNTs is complicated because of their hydrophobic nature.[35] Recent work on mammalian OR protein-based sensors overcame this problem by integrating the ORs into formats that mimic the cell membrane, such as nanovesicles,[1,2,14,16,17] lipid bilayers,[36] and nanodiscs.[4,9] Among these, the OR nanodisc assemblies were found to be stable, and they maintain OR activity over time.[9] The OR nanodisc complex consists of an OR in a nanoscale lipid membrane encapsulated by a membrane scaffold protein (MSP).[9,37] The amine groups on the ORs and MSPs can be used for immobilization of nanodiscs onto the CNTs.

Here, we report the purification of highly sensitive ORs from *Drosophila melanogaster*, their integration into nanodiscs, and fabrication of highly sensitive and selective odorant sensors by immobilizing the OR nanodiscs onto random channel CNT-FETs. Also, we provide the experimental evidence for the selective detection of odorant molecules by OR proteins without the Orco subunit.

EXPERIMENTAL DETAILS

OR Protein Purification and Nanodisc Fabrication and Characterization. The insect odorant receptors were purified as previously described, with some modifications.[38] Briefly, receptor genes were cloned into the pDEST8 vector (ThermoFisher) and transformed into DH10Bac cells to generate bacmids. These bacmids were transfected into Sf9 cells to generate viruses, which were amplified over three passages. The viruses from the third passage (P3) were titred and used to infect Sf9 cells for protein production. The Sf9 cells were maintained in a suspension culture of SF900 II media (ThermoFisher) at 27 °C and 100 rpm. For baculovirus-mediated expression experiments, the cells were diluted to 2×10^6 mL^{-1} and inoculated with virus at a multiplicity of infection (MOI) of 0.1. The odorant receptors were purified from Sf9 cell membranes using standard Ni-NTA and SEC protocols. Briefly, the cells were pelleted, lysed using an Emulsiflex C5 emulsifier (Avestin, Germany) at 10,000−15,000 psi, and centrifuged at ∼100,000*g* for 1 h. The cell pellet was then solubilized in 20 mM tris (pH 7.4), 100 mM NaCl, and 0.5% Fos Choline-14. The sample was centrifuged at ∼100,000*g* for 1 h, and then, the supernatant was purified using a His-Trap column. The protein was further purified with a Superdex 200 pg 16/60 column in 20 mM tris (pH 7.4), 100 mM NaCl, and 0.36 mM Fos Choline-14. The purified protein was concentrated to ∼7 mg/mL with a Vivapsin column (MWCO, 100,000).

The ORs were integrated into nanodiscs based on published protocols.[39] Briefly, the purified OR was incubated with the membrane scaffold protein (MSP1E3D1 (Cube Biotech)) and lipid (POPC) at a molar ratio of 0.2:1:150 for 1 h on ice. Bio-Beads SM-2 (Bio-Rad, USA) were added at 1 mg/mL sample and incubated overnight at 4 °C. The integrated nanodiscs were removed from Bio-Beads and centrifuged at 5000*g* for 5 min to remove aggregates. Zeta potentials of the separated nanodiscs were measured using Zetasizer Nano ZS 90 (Malvern, U.K.). OR nanodiscs were diluted 1:100 (volume ratio) in 1% DMSO in 1× PBS and loaded into a folded capillary zeta cell (DTS1060, Malvern Pananalytical). One hundred measurements were taken for each sample, and measurements were repeated three times to calculate the average result and standard deviations.

CNT-FET Fabrication. CNT-FETs with channel dimensions of 40 μm length and 100 μm width were fabricated using standard photolithography and metal deposition techniques.[40−42] First, CNT thin films were fabricated by a solution processing method directly onto a 100 nm oxide-coated heavily doped p-type silicon substrate (Silicon Quest International, Inc.). CNT bucky paper with 99% semiconducting CNTs (NanoIntegris, IsoNanotubes S-99) was weighed with a high-precision balance (resolution of 0.1 μg) to create 5 μg/mL CNT suspension in anhydrous 1,2-dichlorobenzene (DCB) (99%, Sigma Aldrich) via ultrasonication for 15 min. The water temperature was kept at 25 °C throughout the sonication process. Prior to CNT deposition, a monolayer of 2-mercaptopyridine was deposited onto the SiO_2/Si substrate. A cured polydimethylsiloxane (PDMS) (Sylgard 184) surface was cleaned by 50 W oxygen plasma for 1 min. Ten milligrams of 2-mercaptopyridine (99%, Sigma Aldrich) was dissolved in 1 mL of ethanol and spin-coated onto PDMS at 2000 rpm for 40 s. SiO_2/Si substrates were cleaned in acetone and isopropyl alcohol (IPA) and then dried in nitrogen. The cleaned SiO_2/Si substrates were placed upside down on the PDMS surface for 3 min to functionalize the oxide-coated surface with thiolpyridine. The excess 2-mercaptopyridine on the substrates was removed by washing in absolute ethanol, followed by a nitrogen drying step. The SiO_2/Si substrates were then immersed in CNT suspension for 10 min.[43] After removing the substrates from the suspension, they were dipped into absolute ethanol for another 10 min to remove excess and loosely attached CNT bundles on the surface and dried in nitrogen.

The channel area was defined by standard photolithography, and unwanted areas of the CNT film on the substrates were burned by 200 W oxygen plasma at 600 mTorr for 3 min using a reactive ion etcher (Oxford Instruments, Plasmalab 80 Plus). Successive deposition of 5 nm chromium and 50 nm gold layer was used to define the drain and source electrodes using a thermal evaporator under high vacuum (2×10^{-6} mTorr), followed by defining of the electrodes by photolithography. Atomic force microscopy (AFM) (Nanosurf, NaioAFM) images of the films were taken in the channel regions of the devices before the electrodes were encapsulated by Photoresist AZ 1518 (MicroChemicals) and hard-baked at 200 °C. The effective channel area open to the environment was 10 μm in length and 100 μm in width after encapsulation.

OR Sensor Fabrication. The sensors were fabricated by immobilizing the OR nanodiscs onto the CNT channel. First, the encapsulated CNT-FETs were immersed in 1 mM 1-pyrenebutanoicacid/succinimidyl ester (PBASE) solution in methanol for 1 h. PBASE solution was prepared by sonicating the required amount of PBASE in methanol for 1 min. The solution was kept at room temperature until a clear solution was observed. The devices were washed three times in methanol and subsequently washed three times in PBS to remove the excess PBASE and residual methanol in the channel. The OR nanodiscs were diluted 1:100 with 1× PBS (pH 7.4), and 100 μL was placed in the channel and incubated at room temperature for 1 h in a closed Petri dish. After nanodisc functionalization, the devices were gently washed in PBS for 10 s at room temperature.

AFM images were taken after nanodisc immobilization to confirm the functionalization. To do so, the buffer solution remaining on the device after functionalization was drained, and the device was dried in nitrogen. The active device channels were then imaged using AFM (Nanosurf, NaioAFM) in tapping mode.

Electrical Measurements of CNT-FETs and Sensors. Electrical measurements were carried out using top liquid-gated geometry with 1× PBS (pH 7.4) as the electrolyte. A custom-made PDMS well was used to keep the electrolyte and analytes on the channel. All electrical measurements were carried out at room temperature using a parameter analyzer (Agilent 4156C) and a Rucker and Kolls probe station with micromanipulators. A Ag/AgCl reference electrode

DOI: 10.1021/acsami.8b19433
ACS Appl. Mater. Interfaces 2019, 11, 9530−9538

(BASi) was used as the gate electrode. Transfer characteristics of fabricated CNT-FETs and OR nanodisc-immobilized CNT-FET sensors were measured at a constant drain source voltage (V_{ds}) of 100 mV. The liquid gate voltage (V_{lg}) was swept from −0.5 to 1 V with an interval of 20 mV, and drain source current (I_{ds}) was measured.

The OR nanodisc-immobilized device with a PDMS well mounted on it was placed onto the probe station, and source and drain connections were made by micromanipulators. PBS buffer (100 μL) containing 1% DMSO was added to the well, and the Ag/AgCl standard electrode was placed into the buffer. The ligands were prepared by dissolving in PBS buffer containing 1% DMSO. Ligand solution was added to the well at 5 min intervals to make final concentrations from 1 fM to 10 pM. Real-time sensor measurement was carried out by continuously measuring I_{ds} at an interval of 1 s.

RESULTS AND DISCUSSION

OR Nanodiscs. We recombinantly expressed and purified four insect ORs (DmelOR10a, DmelOR22a, DmelOR35a, and DmelOR71a) using a baculovirus-mediated Sf9 cell system.[38] These proteins were concentrated to ∼7 mg/mL and incorporated into nanodiscs using the membrane scaffold protein MSP1E3D1 and lipid POPC. Table 1 summarizes the ORs used in this study and the positive and negative ligands tested for each OR.[31,44,45]

Table 1. Positive and Negative Ligands for ORs Used in This Work

OR	positive ligand	negative ligand
DmelOR10a (OR10a)	methyl salicylate (MeSal)	E2-Hex
DmelOR22a (OR22a)	methyl hexanoate (MeHex)	E2-Hex
DmelOR35a (OR35a)	*trans*-2-hexen-1-al (E2-Hex)	MeHex
DmelOR71a (OR71a)	4-ethylguaiacol (4EG)	E2-Hex

The zeta potentials of the OR nanodiscs in Table 1 were investigated to understand the charged nature of nanodiscs and their influence in our devices. Zeta potentials were measured using Zetasizer Nano ZS 90 (Malvern, U.K.). One hundred measurements were taken for each sample, and measurements were repeated three times to calculate the average and standard deviations. Table 2 summarizes the zeta potentials of the OR nanodiscs. All the nanodisc samples showed negative zeta potentials, demonstrating that they have a negative surface charge.

Table 2. Zeta Potentials of Nanodisc Dispersion in 1× PBS Containing 1% DMSO

OR nanodisc	zeta potential (mV)
OR10a	−6.67 ± 0.94
OR22a	−6.01 ± 0.44
OR35a	−5.84 ± 0.83
OR71a	−5.67 ± 0.60
empty nanodiscs	−5.02 ± 0.25

OR Nanodisc Functionalization. The immobilization of OR nanodiscs onto the sidewalls of CNTs was carried out via a noncovalent functionalization technique, as described in Experimental Details. First, the 1-pyrenebutanoic acid succinimidyl ester (PBASE) molecules were attached noncovalently onto the CNT sidewalls by dipping the devices into 1 mM PBASE solution in methanol for 1 h.[42,46] This resulted in a stacking of PBASE molecules onto the sidewalls of the CNT via a $\pi-\pi$ interaction between the hexagonal carbon rings of the CNTs and the pyrene group on the PBASE molecule.[42,47] Then, the amine groups on the proteins in the nanodiscs were anchored onto the *N*-hydroxysuccinimide ester group on the PBASE molecule via a nucleophilic substitution reaction.[47] To confirm the functionalization of nanodiscs onto the CNT network, we imaged the CNT thin films with AFM before and after immobilizing the nanodiscs. As shown in Figure 1a, the pristine CNT film contains multitube CNT bundles with varying lengths and diameters. The AFM image confirms that the empty nanodiscs were selectively functionalized on the CNT bundles. Figure 1b−e shows the immobilization of OR10a, OR22a, OR35a, and OR71a nanodiscs, respectively, on the sensor surface. Figure 1f shows the empty nanodisc-immobilized CNT film. Large clusters with varying diameters were observed frequently on the CNT film after nanodisc functionalization for OR10a and OR35a samples and, infrequently, although some were visible, for OR22a, OR71a, and empty nanodiscs. These clusters appear to be formed by agglomeration of the smaller nanodiscs of varying sizes. An indication of this is shown in the transmission electron microscope images given in Figure S1, where only large clusters of nanodiscs were found for an OR35a solution. The nanodiscs are tethered preferentially along the CNT bundles, and no nanodiscs or clusters were found on the substrate.

Electrical Measurements of Sensors. The transfer characteristics of fabricated CNT-FETs and nanodisc-immobilized sensors were also measured to ensure functionalization. As described in Experimental Details, the measurements were carried out in 1× phosphate-buffered saline (PBS, pH 7.4) containing 1% DMSO with a Ag/AgCl electrode as the gate electrode.[48] Figure 2 shows the transfer characteristic curves of CNT-FETs before and after nanodisc immobilization. All pristine CNT-FETs showed ambipolarity, which is consistent with previously reported random CNT network FETs. Gating was achieved at low voltages because of the high effective capacitance of the electrical double layer (EDL) formed around the CNTs in liquid-gated devices.[49,50] Also, CNT-FETs showed a positive threshold voltage (V_{th}), which indicates the hole-dominated charge transport across the channel at V_{lg} = 0 V.

The functionalization of all four OR nanodiscs and empty nanodiscs resulted in similar changes in the transfer characteristics of the CNT-FETs (Figure 2). The threshold voltage of the CNT-FET experienced a considerable negative shift after nanodisc functionalization, regardless of which receptor protein was integrated. We can confirm that the negative shift in the threshold only occurs after the functionalization of the OR nanodisc and is not due to the PBASE functionalization step (see Figure S2 for transfer curves of a pristine, PBASE, and OR71a nanodisc-functionalized CNT network FET). These results are consistent with other reports on protein-immobilized CNT-FETs, which also demonstrate a negative threshold voltage shift after protein immobilization.[9,35,51−54] The V_{th} shift indicates that the immobilization of nanodiscs causes either a positively charged gating effect around the CNTs or injection of electrons to the CNT network, which results in a reduction in the number of holes in the network. However, the electrostatic gating effect can be observed only if the external charges are tethered within the Debye screening length (λ_D) of the electrolyte,[42,55] and as shown in Table 2, the zeta potential values are negative for all the OR nanodiscs including the empty nanodiscs. The

DOI: 10.1021/acsami.8b19433
ACS Appl. Mater. Interfaces 2019, 11, 9530−9538

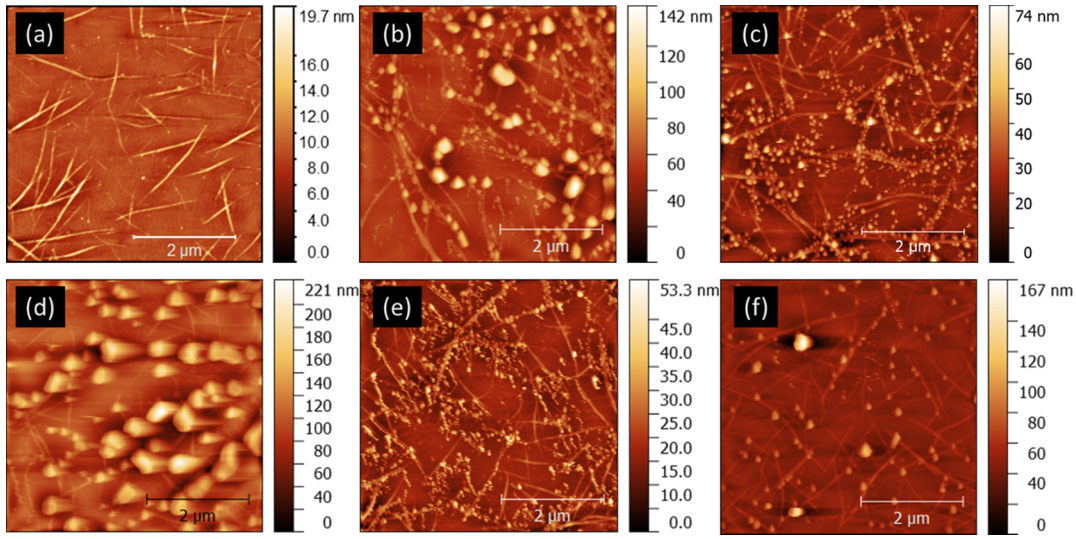

Figure 1. AFM images of (a) pristine, (b) OR10a, (c) OR22a, (d) OR35a, (e) OR71a, and (f) empty nanodiscs immobilized onto CNT films.

functionalization of the nanodisc immobilized onto the CNTs based on the AFM images is represented schematically in Figure 3. The OR proteins and MSPs both contain amine groups; thus, the OR nanodiscs can be tethered to PBASE-functionalized CNTs either with the amine groups on the OR itself or with the amine groups on the MSP. The λ_D of 1× PBS buffer is approximately 0.7 nm,[55−57] and the average height of the nanodiscs used in our study is between 10 to 35 nm, which means that the nanodiscs extend significantly above λ_D on the CNT sidewalls after functionalization. Previous studies reported that proteins are capable of donating electrons from their amine group when they are tethered onto the CNTs.[52,53] We postulate that the negative shift in the threshold voltage in our system is due to an injection of electrons that subsequently reduces the number of holes in the CNT network, which is similar to previous studies.[9,35,51−54] However, the p-type behavior of the CNT network FETs at V_{lg} = 0 V is preserved after nanodisc functionalization, which indicates that the holes are the dominating charge carriers in conduction at V_{lg} = 0 V even after nanodisc tethering. In addition to the negative threshold voltage shift, the on-current and on−off ratio also increased after nanodisc functionalization. We attribute this to changes at the CNT−CNT junctions after nanodisc functionalization due to charge redistribution in the CNT network. The gating of CNT network FETs is dominated by the modulation of Schottky barriers at the metallic and semiconducting CNT junctions throughout the network.[43,58,59] Because of the injection of electrons to the CNT network during OR nanodisc functionalization,[53,60,61] the Fermi levels of CNTs are expected to change, subsequently altering the Schottky barrier height at the CNT−CNT junctions. We hypothesize that the increased on−off ratio we observed is due to these changes in Schottky barrier height, making the gating far more effective across the entire CNT network device, resulting in improved FET performance after OR functionalization.

Sensor Characterization. After nanodisc functionalization, the sensors were tested against their positive ligand and a selected negative ligand, as summarized in Table 1. The measurements were carried out under 0 V liquid gate bias (V_{lg}) and V_{ds} = 100 mV. The current (I_{ds}) through the device was continuously measured at 1 s intervals using a parameter analyzer with a current preamplifier. The normalized current responses of all four CNT-FET OR sensors and those tested against their corresponding positive ligands are shown in Figure 4. The current through the devices (I_{ds}) decreased rapidly upon addition of the respective positive ligand for each OR. We added the additional ligands to the sensing well at a set time interval of 5 min for all sensors tested. As in Figure 4, the response of OR10a, OR22a, and OR71a nanodisc sensors appear to be stabilized within 5 min. However, the sensing responses of OR35a nanodisc-based sensors are less stable within this time interval, and we note that these results may be less definitive than the other three sensors tested. At this point, we also note that the AFM scan showed large clusters of OR nanodisc material for the OR35a samples, and poorer device stability could be due to these clusters. We have repeated each of the experiments three times to avoid as many uncertainties as possible during the sensor measurements, and these collated results are discussed below.

We have also measured the current response of OR nanodisc-immobilized CNT-FET sensors to the corresponding negative ligand (as listed in Table 1). Figure 5 summarizes the sensor performance of three identical sensors for both positive and negative ligands for each receptor used. The response of empty nanodiscs to each ligand is also shown as a further negative control. The error bars in Figure 5 are determined from the sensing responses of three identical sensors tested under identical conditions. The empty nanodisc sensors show no significant change in I_{ds} during ligand addition. Regardless of the ligands used, the empty nanodisc sensors showed a maximum average response of less than 4% for ligands at the highest concentration tested of 10 pM. This response is less than that of OR nanodisc sensors for their corresponding positive ligand, at concentrations four orders of magnitude less concentrated, at 1 fM and is similar to the response of OR nanodisc sensors to their negative ligands. The dose-dependent response for the positive ligands is clearly observed in all four OR nanodisc-immobilized sensors and follows the Langmuir model for ligand−receptor interactions (see Figure S3).[62] We demonstrated that OR-immobilized CNT-FET sensors can respond to their odorants at concentrations as low as 1 fM. This is comparable with the recent mammalian OR-based odorant sensors, as shown in Table S1. The sensors showed an

DOI: 10.1021/acsami.8b19433
ACS Appl. Mater. Interfaces 2019, 11, 9530−9538

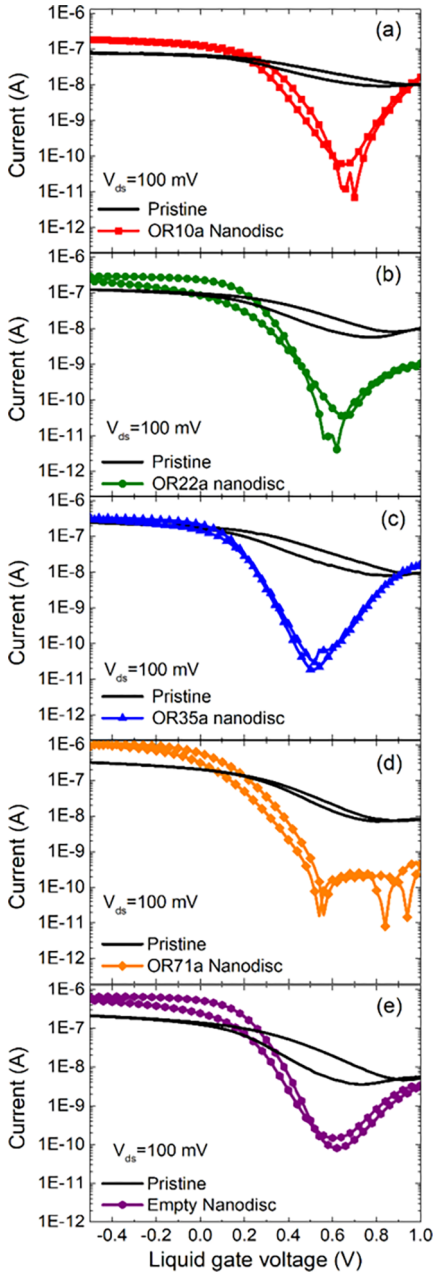

Figure 2. Transfer characteristic curves of CNT network FETs before and after functionalization with (a) OR10a, (b) OR22a, (c) OR35a, (d) OR71a, and (e) empty nanodiscs.

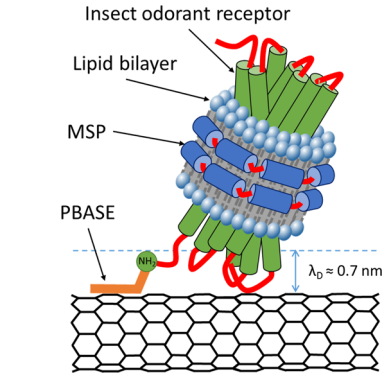

Figure 3. Schematic of OR nanodiscs immobilized on a CNT. λ_D is the Debye screening length of 1× PBS (not drawn to scale).

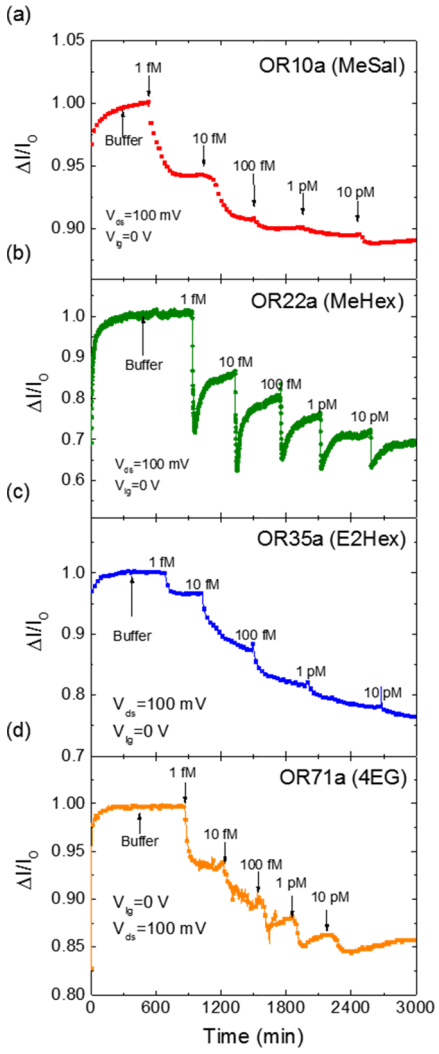

Figure 4. Normalized real-time response to the addition of various concentrations of corresponding positive ligands of (a) OR10a, (b) OR22a, (c) OR35a, and (d) OR71a nanodisc-immobilized CNT-FET sensors.

initial decrement of ∼15% for OR22a and ∼5% for the other three ORs (OR10a, OR35a, and OR71a) after the addition of 1 fM positive ligand. Each of the OR sensors showed lower responses (1 to 2%) in I_{ds} when they are exposed to the selected 1 fM negative ligand. From these results, we can conclude that the OR nanodiscs selectively respond to specific odorants. As shown in Figure 5, the average magnitude of the sensor response is dependent on the OR. It can be seen that OR22a nanodisc sensors showed the largest response to the corresponding positive ligand, whereas the other three showed similar responses that are only one-third of the magnitude of the OR22a sensor. For all of our repeated measurements, we tested three individual sensor devices fabricated to be as similar as possible to take into account the effects introduced by the CNT platform on the sensor performance. This allows us to say that the difference in signal strength across our devices is due to the receptor and not the sensor platform. However, understanding the variation in the magnitude of the electrical response between four different OR nanodisc sensors will

DOI: 10.1021/acsami.8b19433
ACS Appl. Mater. Interfaces 2019, 11, 9530−9538

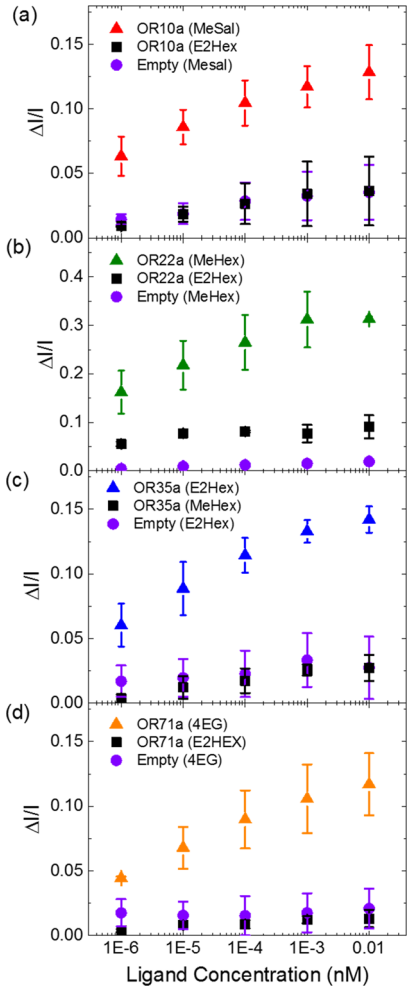

Figure 5. Summary of normalized sensitivity of corresponding positive (triangles) and negative (squares) ligands with (a) OR10a, (b) OR22a, (c) OR35a, and (d) OR71a nanodiscs and response of the corresponding positive ligand to empty nanodisc (circles)-immobilized CNT-FET sensors. The error bars are from three replicates for each sensing test.

require further studies on the structural and electrical properties of the ORs used.

Sensing Mechanism. The reduction in I_{ds} during positive ligand addition demonstrates that an electrical change has occurred in the ORs during odorant binding. However, the structural and electrical changes taking place in insect ORs during sensing are unknown. We can begin to explain the reduction in I_{ds} during ligand addition by considering the CNT-FET response. We measured the transfer characteristics of the OR sensors 5 min after the addition of *trans*-2-hexen-1-ol to an OR35a nanodisc-immobilized sensor (Figure 6), demonstrating that the threshold voltages shift negatively after the addition of a positive ligand. As we discussed earlier, the reduction in I_{ds} in CNT-FETs is due to either electrostatic gating by an isolated positive charge within the Debye screening length from the channel surface or an injection of negative charge to the CNT network. Electrostatic gating effects are not significant in these devices because the λ_D of the buffer used (0.7 nm) during our measurements is much smaller than the height of the immobilized nanodiscs. Therefore, the reduction of I_{ds} in the CNT-FET during ligand addition is more likely to be due to the addition of electrons to the CNT

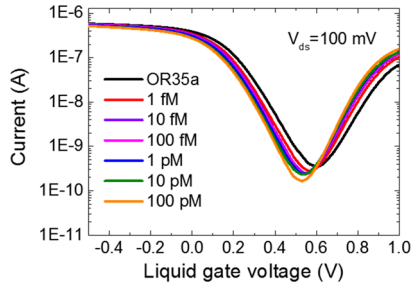

Figure 6. Transfer characteristic curves of an OR35a nanodisc-immobilized CNT-FET sensor after addition of increasing concentrations (1 fM to 100 pM) of *trans*-2-hexen-1-al, showing a reduction in the threshold voltage.

network. It is also likely that structural changes in the OR protein creates an extra negative charge in the restructured protein, which is then transferred to the CNT network and subsequently causes a negative shift in the threshold voltage.

An important observation made here is that, in vivo, the insect requires the Orco subunit to be present for a signal to be generated upon ligand binding on the OR.[63−65] Recent cell-based biosensors have also required the Orco subunit to be present.[8,66−68] However, we have shown that the Orco subunit is not necessary in our biosensor, providing experimental evidence that the OR subunit can bind and signal in the absence of Orco or other downstream signaling mechanisms.[64,69,70] Recently, *D. melanogaster* ORs integrated into liposomes without the Orco subunit have been coupled to gold electrodes and demonstrated femtomolar detection of odorants measured by electrochemical impedance spectroscopy.[71]

CONCLUSIONS

We have successfully demonstrated a proof-of-concept biosensor capable of detecting the binding of odorant molecules to insect olfactory receptor proteins integrated into nanodiscs and immobilized on random CNT network FETs. Four ORs from the fruit fly *D. melanogaster* were successfully purified, integrated into nanodiscs, and functionalized onto the CNT sidewalls. The sensors showed excellent sensitivity to their corresponding positive ligands at concentrations of 1 fM, and no response was observed in sensors functionalized with empty nanodiscs. We have also demonstrated that, in a liquid-gated CNT-FET sensor, the Orco subunit is not necessary for signal generation upon cognate ligand binding. This is an exciting discovery because it means that the complete OR-Orco ion channel is not necessary to develop an OR biosensor.

ASSOCIATED CONTENT

Supporting Information

The Supporting Information is available free of charge on the ACS Publications website at DOI: 10.1021/acsami.8b19433.

TEM images of OR35a nanodiscs and comparison of the sensitivity of recent mammalian OR and CNT-FET-based odorant sensors (PDF)

AUTHOR INFORMATION

Corresponding Authors

*E-mail: Colm.Carraher@plantandfood.co.nz (C.C.).
*E-mail: natalie.plank@vuw.ac.nz (N.O.V.P.).

DOI: 10.1021/acsami.8b19433
ACS Appl. Mater. Interfaces 2019, 11, 9530−9538

ORCID

Thanihaichelvan Murugathas: 0000-0002-0481-3194
Colm Carraher: 0000-0001-5341-116X
Natalie O. V. Plank: 0000-0002-9798-9657

Funding

This work was supported by funding awarded to Dr. Colm Carraher through a Royal Society Rutherford Postdoctoral Scholarship (RFT-PAF1501-PD) and a Marsden Fund grant (PAF1503), to Dr. Natalie Plank by the MacDiarmid Institute for Advanced Materials and Nanotechnology, and to Dr. Andrew Kralicek through the Kiwi Innovation Network (KiwiNET) Inaugural Emerging Innovator Award. Murugathas Thanihaichelvan's Ph.D. scholarship was covered by the Marsden Fund grant.

Notes

The authors declare no competing financial interest.

REFERENCES

(1) Son, M.; Cho, D.-g.; Lim, J. H.; Park, J.; Hong, S.; Ko, H. J.; Park, T. H. Real-Time Monitoring of Geosmin and 2-Methylisoborneol, Representative Odor Compounds in Water Pollution Using Bioelectronic Nose with Human-like Performance. *Biosens. Bioelectron.* **2015**, *74*, 199−206.

(2) Park, J.; Lim, J. H.; Jin, H. J.; Namgung, S.; Lee, S. H.; Park, T. H.; Hong, S. A Bioelectronic Sensor Based on Canine Olfactory Nanovesicle−Carbon Nanotube Hybrid Structures for the Fast Assessment of Food Quality. *Analyst* **2012**, *137*, 3249−3254.

(3) Lim, J. H.; Park, J.; Ahn, J. H.; Jin, H. J.; Hong, S.; Park, T. H. A Peptide Receptor-Based Bioelectronic Nose for the Real-Time Determination of Seafood Quality. *Biosens. Bioelectron.* **2013**, *39*, 244−249.

(4) Yang, H.; Kim, D.; Kim, J.; Moon, D.; Song, H. S.; Lee, M.; Hong, S.; Park, T. H. Nanodisc-Based Bioelectronic Nose Using Olfactory Receptor Produced in *Escherichia coli* for the Assessment of the Death-Associated Odor Cadaverine. *ACS Nano* **2017**, *11*, 11847−11855.

(5) Lim, J. H.; Park, J.; Oh, E. H.; Ko, H. J.; Hong, S.; Park, T. H. Nanovesicle-Based Bioelectronic Nose for the Diagnosis of Lung Cancer from Human Blood. *Adv. Healthcare Mater.* **2014**, *3*, 360−366.

(6) Oh, Y.; Lee, Y.; Heath, J.; Kim, M. Applications of Animal Biosensors: A Review. *IEEE Sens. J.* **2015**, *15*, 637−645.

(7) Leitch, O.; Anderson, A.; Kirkbride, K. P.; Lennard, C. Biological Organisms as Volatile Compound Detectors: A Review. *Forensic Sci. Int.* **2013**, *232*, 92−103.

(8) Mitsuno, H.; Sakurai, T.; Namiki, S.; Mitsuhashi, H.; Kanzaki, R. Novel Cell-Based Odorant Sensor Elements Based on Insect Odorant Receptors. *Biosens. Bioelectron.* **2015**, *65*, 287−294.

(9) Goldsmith, B. R.; Mitala, J. J., Jr.; Josue, J.; Castro, A.; Lerner, M. B.; Bayburt, T. H.; Khamis, S. M.; Jones, R. A.; Brand, J. G.; Sligar, S. G.; Luetje, C. W.; Gelperin, A.; Paul, A. R.; Bohdana, M. D.; Johnson, A. T. C. Biomimetic Chemical Sensors Using Nanoelectronic Readout of Olfactory Receptor Proteins. *ACS Nano* **2011**, *5*, 5408−5416.

(10) Lee, S. H.; Jin, H. J.; Song, H. S.; Hong, S.; Park, T. H. Bioelectronic Nose with High Sensitivity and Selectivity Using Chemically Functionalized Carbon Nanotube Combined with Human Olfactory Receptor. *J. Biotechnol.* **2012**, *157*, 467−472.

(11) Zhang, A.; Lieber, C. M. Nano-Bioelectronics. *Chem. Rev.* **2016**, *116*, 215−257.

(12) Liu, S.; Guo, X. Carbon Nanomaterials Field-Effect-Transistor-Based Biosensors. *NPG Asia Mater.* **2012**, *4*, No. e23.

(13) Yang, N.; Chen, X.; Ren, T.; Zhang, P.; Yang, D. Carbon Nanotube Based Biosensors. *Sens. Actuators, B* **2015**, *207*, 690−715.

(14) Jin, H. J.; Lee, S. H.; Kim, T. H.; Park, J.; Song, H. S.; Park, T. H.; Hong, S. Nanovesicle-Based Bioelectronic Nose Platform Mimicking Human Olfactory Signal Transduction. *Biosens. Bioelectron.* **2012**, *35*, 335−341.

(15) Park, S. J.; Kwon, O. S.; Lee, S. H.; Song, H. S.; Park, T. H.; Jang, J. Ultrasensitive Flexible Graphene Based Field-Effect Transistor (FET)-Type Bioelectronic Nose. *Nano Lett.* **2012**, *12*, 5082−5090.

(16) Lim, J. H.; Oh, E. H.; Park, J.; Hong, S.; Park, T. H. Ion-Channel-Coupled Receptor-Based Platform for a Real-Time Measurement of G-Protein-Coupled Receptor Activities. *ACS Nano* **2015**, *9*, 1699−1706.

(17) Ahn, J. H.; Lim, J. H.; Park, J.; Oh, E. H.; Son, M.; Hong, S.; Park, T. H. Screening of Target-Specific Olfactory Receptor and Development of Olfactory Biosensor for the Assessment of Fungal Contamination in Grain. *Sens. Actuators, B* **2015**, *210*, 9−16.

(18) Park, S. J.; Lee, S. H.; Yang, H.; Park, C. S.; Lee, C.-S.; Kwon, O. S.; Park, T. H.; Jang, J. Human Dopamine Receptor-Conjugated Multidimensional Conducting Polymer Nanofiber Membrane for Dopamine Detection. *ACS Appl. Mater. Interfaces* **2016**, *8*, 28897−28903.

(19) Son, M.; Kim, D.; Kang, J.; Lim, J. H.; Lee, S. H.; Ko, H. J.; Hong, S.; Park, T. H. Bioelectronic Nose Using Odorant Binding Protein-Derived Peptide and Carbon Nanotube Field-Effect Transistor for the Assessment of *Salmonella* Contamination in Food. *Anal. Chem.* **2016**, *88*, 11283−11287.

(20) Kwon, O. S.; Song, H. S.; Park, S. J.; Lee, S. H.; An, J. H.; Park, J. W.; Yang, H.; Yoon, H.; Bae, J.; Park, T. H.; Jang, J. An Ultrasensitive, Selective, Multiplexed Superbioelectronic Nose That Mimics the Human Sense of Smell. *Nano Lett.* **2015**, *15*, 6559−6567.

(21) Kaupp, U. B. Olfactory Signalling in Vertebrates and Insects: Differences and Commonalities. *Nat. Rev. Neurosci.* **2010**, *11*, 188−200.

(22) Quignon, P.; Kirkness, E.; Cadieu, E.; Touleimat, N.; Guyon, R.; Renier, C.; Hitte, C.; André, C.; Fraser, C.; Galibert, F. Comparison of the Canine and Human Olfactory Receptor Gene Repertoires. *Genome Biol.* **2003**, *4*, R80.

(23) Persaud, K.; Dodd, G. Analysis of Discrimination Mechanisms in the Mammalian Olfactory System Using a Model Nose. *Nature* **1982**, *299*, 352−355.

(24) Neuhaus, E. M.; Gisselmann, G.; Zhang, W.; Dooley, R.; Störtkuhl, K.; Hatt, H. Odorant Receptor Heterodimerization in the Olfactory System of *Drosophila melanogaster*. *Nat. Neurosci.* **2005**, *8*, 15−17.

(25) German, P. F.; van der Poel, S.; Carraher, C.; Kralicek, A. V.; Newcomb, R. D. Insights into Subunit Interactions within the Insect Olfactory Receptor Complex Using FRET. *Insect Biochem. Mol. Biol.* **2013**, *43*, 138−145.

(26) Jones, P. L.; Pask, G. M.; Rinker, D. C.; Zwiebel, L. J. Functional Agonism of Insect Odorant Receptor Ion Channels. *Proc. Natl. Acad. Sci. U. S. A.* **2011**, *108*, 8821−8825.

(27) Carraher, C.; Dalziel, J.; Jordan, M. D.; Christie, D. L.; Newcomb, R. D.; Kralicek, A. V. Towards an Understanding of the Structural Basis for Insect Olfaction by Odorant Receptors. *Insect Biochem. Mol. Biol.* **2015**, *66*, 31−41.

(28) Sánchez-Gracia, A.; Vieira, F. G.; Rozas, J. Molecular Evolution of the Major Chemosensory Gene Families in Insects. *Heredity* **2009**, *103*, 208−216.

(29) McBride, C. S. Rapid Evolution of Smell and Taste Receptor Genes during Host Specialization in *Drosophila sechellia*. *Proc. Natl. Acad. Sci. U. S. A.* **2007**, *104*, 4996−5001.

(30) McBride, C. S.; Arguello, J. R. Five Drosophila Genomes Reveal Nonneutral Evolution and the Signature of Host Specialization in the Chemoreceptor Superfamily. *Genetics* **2007**, *177*, 1395−1416.

(31) Hallem, E. A.; Carlson, J. R. Coding of Odors by a Receptor Repertoire. *Cell* **2006**, *125*, 143−160.

(32) Boyle, S. M.; McInally, S.; Ray, A. Expanding the Olfactory Code by in Silico Decoding of Odor-Receptor Chemical Space. *eLife* **2013**, *2*, No. e01120.

(33) Mathew, D.; Martelli, C.; Kelley-Swift, E.; Brusalis, C.; Gershow, M.; Samuel, A. D. T.; Emonet, T.; Carlson, J. R. Functional

DOI: 10.1021/acsami.8b19433
ACS Appl. Mater. Interfaces 2019, 11, 9530−9538

Diversity among Sensory Receptors in a *Drosophila* Olfactory Circuit. *Proc. Natl. Acad. Sci.* **2013**, *110*, E2134−E2143.
(34) Couto, A.; Alenius, M.; Dickson, B. J. Molecular, Anatomical, and Functional Organization of the *Drosophila* Olfactory System. *Curr. Biol.* **2005**, *15*, 1535−1547.
(35) Zhou, X.; Moran-Mirabal, J. M.; Craighead, H. G.; McEuen, P. L. Supported Lipid Bilayer/Carbon Nanotube Hybrids. *Nat. Nanotechnol.* **2007**, *2*, 185−190.
(36) Kim, T. H.; Lee, S. H.; Lee, J.; Song, H. S.; Oh, E. H.; Park, T. H.; Hong, S. Single-Carbon-Atomic-Resolution Detection of Odorant Molecules Using a Human Olfactory Receptor-Based Bioelectronic Nose. *Adv. Mater.* **2009**, *21*, 91−94.
(37) Bayburt, T. H.; Grinkova, Y. V.; Sligar, S. G. Self-Assembly of Discoidal Phospholipid Bilayer Nanoparticles with Membrane Scaffold Proteins. *Nano Lett.* **2002**, *2*, 853−856.
(38) Carraher, C.; Nazmi, A. R.; Newcomb, R. D.; Kralicek, A. Recombinant Expression, Detergent Solubilisation and Purification of Insect Odorant Receptor Subunits. *Protein Expression Purif.* **2013**, *90*, 160−169.
(39) Ritchie, T. K.; Grinkova, Y. V.; Bayburt, T. H.; Denisov, I. G.; Zolnerciks, J. K.; Atkins, W. M.; Sligar, S. G. Reconstitution of Membrane Proteins in Phospholipid Bilayer Nanodiscs. *Methods Enzymol.* **2009**, *464*, 211−231.
(40) Zheng, H. Y.; Plank, N. O. V. Facile Fabrication of Carbon Nanotube Network Thin Film Transistors for Device Platforms. *Int. J. Nanotechnol.* **2017**, *14*, 505.
(41) Plank, N. O. V.; Ishida, M.; Cheung, R. Positioning of Carbon Nanotubes Using Soft-Lithography for Electronics Applications. *J. Vac. Sci. Technol., B: Microelectron. Nanometer Struct.: Process., Meas., Phenom.* **2005**, *23*, 3178.
(42) Zheng, H. Y.; Alsager, O. A.; Zhu, B.; Travas-Sejdic, J.; Hodgkiss, J. M.; Plank, N. O. V. Electrostatic Gating in Carbon Nanotube Aptasensors. *Nanoscale* **2016**, *8*, 13659−13668.
(43) Thanihaichelvan, M.; Browning, L. A.; Dierkes, M. P.; Reyes, R. M.; Kralicek, A. V.; Carraher, C.; Marlow, C. A.; Plank, N. O. V. Metallic-Semiconducting Junctions Create Sensing Hot-Spots in Carbon Nanotube FET Aptasensors near Percolation. *Biosens. Bioelectron.* **2018**, *130*, 408−413, DOI: 10.1016/j.bios.2018.09.021.
(44) Hallem, E. A.; Carlson, J. R. The Odor Coding System of *Drosophila*. *Trends Genet.* **2004**, *20*, 453−459.
(45) Dweck, H. K. M.; Ebrahim, S. A. M.; Farhan, A.; Hansson, B. S.; Stensmyr, M. C. Olfactory Proxy Detection of Dietary Antioxidants in Drosophila. *Curr. Biol.* **2015**, *25*, 455−466.
(46) Zheng, H. Y.; Alsager, O. A.; Wood, C. S.; Hodgkiss, J. M.; Plank, N. O. V. Carbon Nanotube Field Effect Transistor Aptasensors for Estrogen Detection in Liquids. *J. Vac. Sci. Technol., B* **2015**, *33*, No. 06F904.
(47) Star, A.; Liu, Y.; Grant, K.; Ridvan, L.; Stoddart, J. F.; Steuerman, D. W.; Diehl, M. R.; Boukai, A.; Heath, J. R. Noncovalent Side-Wall Functionalization of Single-Walled Carbon Nanotubes. *Macromolecules* **2003**, *36*, 553−560.
(48) Minot, E. D.; Janssens, A. M.; Heller, I.; Heering, H. A.; Dekker, C.; Lemay, S. G. Carbon Nanotube Biosensors: The Critical Role of the Reference Electrode. *Appl. Phys. Lett.* **2007**, *91*, No. 093507.
(49) Heller, I.; Chatoor, S.; Männik, J.; Zevenbergen, M. A. G.; Dekker, C.; Lemay, S. G. Comparing the Weak and Strong Gate-Coupling Regimes for Nanotube and Graphene Transistors. *Phys. Status Solidi RRL* **2009**, *3*, 190−192.
(50) Fujimoto, T.; Awaga, K. Electric-Double-Layer Field-Effect Transistors with Ionic Liquids. *Phys. Chem. Chem. Phys.* **2013**, *15*, 8983−9006.
(51) Lerner, M. B.; Goldsmith, B. R.; McMillon, R.; Dailey, J.; Pillai, S.; Singh, S. R.; Johnson, A. T. C. A Carbon Nanotube Immunosensor for *Salmonella*. *AIP Adv.* **2011**, *1*, No. 042127.
(52) Heller, I.; Janssens, A. M.; Männik, J.; Minot, E. D.; Lemay, S. G.; Dekker, C. Identifying the Mechanism of Biosensing with Carbon Nanotube Transistors. *Nano Lett.* **2008**, *8*, 591−595.
(53) Bradley, K.; Briman, M.; Star, A.; Grüner, G. Charge Transfer from Adsorbed Proteins. *Nano Lett.* **2004**, *4*, 253−256.
(54) Star, A.; Gabriel, J.-C. P.; Bradley, K.; Grüner, G. Electronic Detection of Specific Protein Binding Using Nanotube FET Devices. *Nano Lett.* **2003**, *3*, 459−463.
(55) Stern, E.; Wagner, R.; Sigworth, F. J.; Breaker, R.; Fahmy, T. M.; Reed, M. A. Importance of the Debye Screening Length on Nanowire Field Effect Transistor Sensors. *Nano Lett.* **2007**, *7*, 3405−3409.
(56) Lin, S.-P.; Pan, C.-Y.; Tseng, K.-C.; Lin, M.-C.; Chen, C.-D.; Tsai, C.-C.; Yu, S.-H.; Sun, Y.-C.; Lin, T.-W.; Chen, Y.-T. A Reversible Surface Functionalized Nanowire Transistor to Study Protein-Protein Interactions. *Nano Today* **2009**, *4*, 235−243.
(57) Chen, K.-I.; Li, B.-R.; Chen, Y.-T. Silicon Nanowire Field-Effect Transistor-Based Biosensors for Biomedical Diagnosis and Cellular Recording Investigation. *Nano Today* **2011**, *6*, 131−154.
(58) Lee, E. J. H.; Balasubramanian, K.; Burghard, M.; Kern, K. Spatially Resolved Potential Distribution in Carbon Nanotube Cross-Junction Devices. *Adv. Mater.* **2009**, *21*, 2720−2724.
(59) Stadermann, M.; Papadakis, S. J.; Falvo, M. R.; Novak, J.; Snow, E.; Fu, Q.; Liu, J.; Fridman, Y.; Boland, J. J.; Superfine, R.; et al. Nanoscale Study of Conduction through Carbon Nanotube Networks. *Phys. Rev. B: Condens. Matter Mater. Phys.* **2004**, *69*, 201402.
(60) Bradley, K.; Gabriel, J.-C. P.; Briman, M.; Star, A.; Grüner, G. Charge Transfer from Ammonia Physisorbed on Nanotubes. *Phys. Rev. Lett.* **2003**, *91*, 218301.
(61) Chang, H.; Lee, J. D.; Lee, S. M.; Lee, Y. H. Adsorption of NH_3 and NO_2 Molecules on Carbon Nanotubes. *Appl. Phys. Lett.* **2001**, *79*, 3863−3865.
(62) Larisika, M.; Kotlowski, C.; Steininger, C.; Mastrogiacomo, R.; Pelosi, P.; Schütz, S.; Peteu, S. F.; Kleber, C.; Reiner-Rozman, C.; Nowak, C.; et al. Electronic Olfactory Sensor Based on *A. mellifera* Odorant-Binding Protein 14 on a Reduced Graphene Oxide Field-Effect Transistor. *Angew. Chem., Int. Ed.* **2015**, *54*, 13245−13248.
(63) Smart, R.; Kiely, A.; Beale, M.; Vargas, E.; Carraher, C.; Kralicek, A. V.; Christie, D. L.; Chen, C.; Newcomb, R. D.; Warr, C. G. *Drosophila* Odorant Receptors Are Novel Seven Transmembrane Domain Proteins That Can Signal Independently of Heterotrimeric G Proteins. *Insect Biochem. Mol. Biol.* **2008**, *38*, 770−780.
(64) Wicher, D.; Schäfer, R.; Bauernfeind, R.; Stensmyr, M. C.; Heller, R.; Heinemann, S. H.; Hansson, B. S. *Drosophila* Odorant Receptors Are Both Ligand-Gated and Cyclic-Nucleotide- Activated Cation Channels. *Nature* **2008**, *452*, 1007−1011.
(65) Sato, K.; Pellegrino, M.; Nakagawa, T.; Nakagawa, T.; Vosshall, L. B.; Touhara, K. Insect Olfactory Receptors Are Heteromeric Ligand-Gated Ion Channels. *Nature* **2008**, *452*, 1002−1006.
(66) Terutsuki, D.; Mitsuno, H.; Sakurai, T.; Okamoto, Y.; Tixier-Mita, A.; Toshiyoshi, H.; Mita, Y.; Kanzaki, R. Increasing Cell−Device Adherence Using Cultured Insect Cells for Receptor-Based Biosensors. *R. Soc. Open Sci.* **2018**, *5*, 172366.
(67) Termtanasombat, M.; Mitsuno, H.; Misawa, N.; Yamahira, S.; Sakurai, T.; Yamaguchi, S.; Nagamune, T.; Kanzaki, R. Cell-Based Odorant Sensor Array for Odor Discrimination Based on Insect Odorant Receptors. *J. Chem. Ecol.* **2016**, *42*, 716−724.
(68) Misawa, N.; Mitsuno, H.; Kanzaki, R.; Takeuchi, S. Highly Sensitive and Selective Odorant Sensor Using Living Cells Expressing Insect Olfactory Receptors. *Proc. Natl. Acad. Sci. U. S. A.* **2010**, *107*, 15340−15344.
(69) Große-Wilde, E.; Svatoš, A.; Krieger, J. A Pheromone-Binding Protein Mediates the Bombykol-Induced Activation of a Pheromone Receptor in Vitro. *Chem. Senses* **2006**, *31*, 547−555.
(70) Große-Wilde, E.; Gohl, T.; Bouché, E.; Breer, H.; Krieger, J. Candidate Pheromone Receptors Provide the Basis for the Response of Distinct Antennal Neurons to Pheromonal Compounds. *Eur. J. Neurosci.* **2007**, *25*, 2364−2373.
(71) Khadka, R.; Aydemir, N.; Carraher, C.; Hamiaux, C.; Colbert, D.; Cheema, J.; Malmström, J.; Kralicek, A.; Travas-Sejdic, J. An Ultrasensitive Electrochemical Impedance-Based Biosensor Using

DOI: 10.1021/acsami.8b19433
ACS Appl. Mater. Interfaces 2019, 11, 9530−9538

Insect Odorant Receptors to Detect Odorants. *Biosens. Bioelectron.* **2019**, *126*, 207.

DOI: 10.1021/acsami.8b19433
ACS Appl. Mater. Interfaces 2019, 11, 9530−9538